PHILOSOPHICAL TRANSACTIONS OF THE ROYAL SOCIETY A MATHEMATICAL, PHYSICAL & ENGINEERING SCIENCES

Mass, momentum, Sensible Heat and Latent Heat Budgets for the Lower Atmosphere

P. K. Taylor, A. L. M. Grant, H. Gunther and G. Olbruck

Phil. Trans. R. Soc. Lond. A 1983 **308**, 275-290
doi: 10.1098/rsta.1983.0004

Phil. Trans. R. Soc. Lond. A **308**, 275–290 (1983)
Printed in Great Britain

Mass, momentum, sensible heat and latent heat budgets for the lower atmosphere

By P. K. Taylor†, A. L. M. Grant‡, H. Günther§ and G. Olbrück§

† *Institute of Oceanographic Sciences, Brook Road, Wormley, Godalming, Surrey GU8 5UB, U.K.*
‡ *Meteorological Office, London Road, Bracknell, Berks RG12 2SZ, U.K.*
§ *Deutscher Wetterdienst Seewetteramt, Bernhard Nocht-Strasse 76, Hamburg, F.R.G.*

Radiosonde data from the JASIN meteorological triangle, of sides 200 km, have been used to construct mean budgets of mass, momentum and sensible and latent heat. Typically the atmospheric boundary layer (BL) consisted of a near-neutral subcloud layer and a conditionally unstable cloud layer beneath an inversion. Clouds were cumulus under a stratocumulus layer. Wind shears within the BL were small and the mean vertical motion at the BL top was less than 1 μbar s^{-1}||. Acceleration terms were of similar order (10^{-4} m s^{-2}) to the geostrophic departure, and significant stress within the cloud layer implied convective momentum transport. The latent heat flux dominated the sub-grid-scale vertical heat transfer, being on average nearly constant from the surface to the cloud-layer top. The results emphasize the importance of cloud processes in determining boundary layer structure.

1. Introduction

This paper will consider the structure of the lowest 2 km of the atmosphere at a midlatitude open-ocean site. The observations were obtained during the Joint Air–Sea Interaction Experiment (JASIN) (Pollard *et al.*, this symposium), which took place during July to September 1978, in the Rockall Trough region of the North Atlantic. During the daylight hours of chosen Intensive Radiosonde Days (IRDs), radiosondes were released at one- to two-hour intervals from ships at the corners of a triangle of approximately 200 km sides. These data have been used to construct budgets of mass, momentum and thermodynamic energy, which represent the mean atmospheric state over the 200 km area and over time periods of several hours. The vertical sub-grid-scale fluxes of momentum and thermodynamic energy have been calculated from the budget residuals. The region of the atmosphere through which sub-grid-scale fluxes from the sea surface were significant will be termed the atmospheric boundary layer (BL). For the days selected for study the BL will be shown to extend up to the main inversion layer at the cloud-layer top. The BL will therefore be considered to consist of subcloud, cloud and inversion layers with the free atmosphere above. Transfer processes into the BL at the air–sea interface have been discussed, for JASIN, by Guymer *et al.* (this symposium) while Nicholls *et al.* (this symposium) discuss the atmospheric structure on smaller space and time scales than those considered here.

Early observations of the wind structure over the ocean (Sheppard *et al.* 1952, Sheppard & Omar 1952, Charnock *et al.* 1956) were single-point measurements and it was necessary to assume that acceleration terms were small when suitably averaged over time. Baroclinicity could not be measured although its importance was inferred (Sheppard *et al.* 1952). Acceleration, baroclinicity and advection have been assessed in budget studies for multi-ship experiments such

|| 1 bar = 10^5 Pa.

as the Atlantic Tradewind Experiment (ATEX) (Augstein *et al.* 1973; Brümmer 1976) the Barbados Oceanographic and Meteorological Experiment (BOMEX) (Holland & Rasmussen 1973; Nitta & Esbensen 1974), and the GARP Atlantic Tropical Experiment (GATE) (Brümmer 1978). However, each of these was conducted in tropical, sub-tropical or trade-wind conditions. The midlatitude JASIN area is characterized by lower air and sea temperatures and great variability in the synoptic-scale flow. Changes in the BL structure during JASIN associated with the fronts accompanying midlatitude depressions have been discussed by Taylor & Guymer and Guymer *et al.* (this symposium). The lower temperatures, and hence lower saturation water vapour content, might be expected to reduce the importance of moisture in determining boundary layer structure in midlatitudes. However, by presenting in detail the results for one day, 31 August 1978 (§ 4), it will be shown that this was not so. These results will then be compared with values for four other days (§ 5); but first the data and calculation methods will be described.

(*a*) *Notation*

c_p	specific heat at constant pressure ($240 \times 4.1868\,\mathrm{J\,kg^{-1}\,K^{-1}}$)
f	Coriolis parameter ($1.263 \times 10^{-4}\,\mathrm{s^{-1}} \equiv 60°\,\mathrm{N}$)
F_s, F_{Lq}, F_h	sub-grid-scale vertical fluxes of s, Lq and h (see text)
g	acceleration due to gravity ($9.819\,\mathrm{m\,s^{-2}}$)
h	moist static energy ($= s + Lq$; $\mathrm{J\,kg^{-1}}$)
L	latent heat of evaporation ($\mathrm{J\,kg^{-1}}$)
$L(\mathrm{c}-\mathrm{e})$	net release of latent heat through difference between condensation and evaporation rates ($\mathrm{W\,kg^{-1}}$)
Lq	latent energy (latent heat $L \times$ specific humidity q)
p^*	pressure, $p^* = p_0 - p$, where p is the pressure and p_0 is the surface value
p_i^*	mean inversion pressure
p_τ^*	pressure at which $\tau_x = \tau_y = 0$ was assumed (§ 3 *b*)
Q_R	net radiational heating ($\mathrm{W\,kg^{-1}}$)
s	dry static energy ($= c_p T + gz$; $\mathrm{J\,kg^{-1}}$)
T, T_v	temperature, virtual temperature
u, u_g, v, v_g	observed and geostrophic wind components in the x- and y-directions
u_*	friction velocity
x, y	coordinates on an isobaric surface
z	height
Θ_e, Θ_es	equivalent and saturation equivalent potential temperatures
Θ, Θ_v	potential temperature, virtual potential temperature
ρ	air density
τ_x, τ_y	stress components in the x- and y-directions
τ_0	magnitude of surface stress
ω	mean vertical (p^*) wind component, positive upwards ($\mu\mathrm{bar\,s^{-1}} \approx \mathrm{cm\,s^{-1}}$).

2. Data

Radiosondes were released from the ships M.V. *Gardline Endurer*, H.M.S. *Hecla*, and R.V. *Meteor* at the northwest, northeast and south corners respectively of a triangle of sides 200 km centred at 59° N, 12° W (figure 1). Viz 1223 radiosondes were used, in which the rod thermistor, carbon hygristor and aneroid pressure sensor were sampled sequentially every 0.8 s. Winds were measured

by tracking the balloon with use of Loran-C signals retransmitted by the radiosonde (Taylor 1975). Great care was taken to minimize systematic differences between the ships. All the radiosondes used were obtained as a single batch and the factory sensor calibrations have been used to avoid any systematic biases in the shipboard calibration performed before launch. All data were recorded on magnetic tape with similar Beukers W-3 system LO-CATE ground equipment on each ship, and post-experiment processing was performed at a single site. Errors due to recording

TABLE 1. ACCURACY OF RADIOSONDE SENSORS

variable	sensor	factory-specified accuracy	intercomparison mean bias	intercomparison for 5 mbar layers
temperature	Viz 1366–211	± 0.1 K (r.m.s.)	< 0.05 K	< 0.1 K
relative humidity	Viz 1386–060	$\pm 2\%$ (r.m.s.)	$< 1\%$	5%
pressure	Viz 1292–213	within 1 mbar	—	—
winds	(LO-CATE Loran-C)	—	0.05 ± 0.04 m s^{-1}	0.5 m s^{-1}

Columns 4 and 5 refer to intercomparison radiosonde flights in which two or three ships tracked the same radiosonde. The magnitude of the difference between values from different ships is shown by the mean over all such flights. Column 4 shows the mean difference over entire flights while 5 shows the difference for individual 5 mbar layers. In these columns humidity values given are after correction (Taylor 1982); wind values are for a single component.

and processing the data were evaluated by using intercomparison-period (Pollard *et al.*, this symposium) flights and are shown in table 1 together with factory estimates of the sensor accuracy. Further details of the radiosonde data and processing schemes are given by Taylor (1983). Surface data used has been described by Guymer *et al.* (this symposium).

3. BUDGET CALCULATION

(*a*) *Method of calculation*

The method of calculation of the budgets is described in detail by Taylor (1983) and will only be summarized here. The mean momentum budget equations are:

$$\frac{\mathrm{D}u}{\mathrm{D}t} = f(v - v_g) - g\frac{\partial \tau_x}{\partial p}, \quad \frac{\mathrm{D}v}{\mathrm{D}t} = f(u_g - u) - g\frac{\partial \tau_y}{\partial p}, \tag{1}$$

where

$$\frac{\mathrm{D}}{\mathrm{D}t} \equiv u\frac{\partial}{\partial x} + v\frac{\partial}{\partial y} - \omega\frac{\partial}{\partial p} + \frac{\partial}{\partial t}. \tag{2}$$

The mean vertical motion ω was calculated by integration of the divergence equation. Hence

$$\omega = \int_{p_0}^{p} \left(\frac{\partial u}{\partial x} + \frac{\partial v}{\partial y}\right) \mathrm{d}p + \left.\frac{\mathrm{D}p}{\mathrm{D}t}\right|_0, \tag{3}$$

where the last term, representing ω at the sea surface, was found to be negligible. The geostrophic wind components were calculated from the measured surface pressure gradient (§ 3*b*) and the thermal wind equation: for example,

$$v_g = \frac{1}{f\rho_0}\frac{\partial p}{\partial x} - \frac{1}{f}\int_{p_0}^{p} \frac{1}{\rho T_v}\left(\frac{\partial T_v}{\partial x}\right) \mathrm{d}p, \tag{4}$$

where, here and subsequently, a subscript zero indicates a quantity evaluated at the sea surface. Thus equation (1) can be solved for the sub-grid-scale momentum transfers τ_x and τ_y by integration from the surface stress value τ_0.

The budget equation for dry static energy, s, is

$$\frac{\mathrm{D}s}{\mathrm{D}t} = Q_{\mathrm{R}} + L(\mathrm{c}-\mathrm{e}) - g\frac{\partial F_s}{\partial p}, \tag{5}$$

where the net radiational heating, Q_{R}, and the effects of condensation and evaporation, $L(\mathrm{c}-\mathrm{e})$, will be neglected in calculating F_s. Similarly the condensation/evaporation term will be neglected in calculating F_{Lq} from the latent energy budget

$$\frac{\mathrm{D}(Lq)}{\mathrm{D}t} = -L(\mathrm{c}-\mathrm{e}) - g\frac{\partial F_{Lq}}{\partial p}. \tag{6}$$

Since the neglected terms are likely to be significant in the cloud layer the budget of moist static energy will also be presented:

$$\frac{\mathrm{D}h}{\mathrm{D}t} = Q_{\mathrm{R}} - g\frac{\partial F_h}{\partial p}, \tag{7}$$

with the radiation term calculated by Dr A. Slingo using the method described by Roach & Slingo (1979) and Slingo & Schrecker (1982), this having been verified for JASIN by Schmetz *et al.* (this symposium).

The budgets were calculated for 5 mbar atmospheric layers between the surface and 810 mbar with integration replaced by summation over the layers. The surface values of τ, F_s, F_{Lq}, and F_h were calculated from the bulk aerodynamic formula by the method of Large & Pond (1982). Independent budgets were calculated for four-hour sub-periods within an IRD encompassing on average three radiosonde flights from each ship. Most of these flights were tracked both during ascent and parachute descent after release of the balloon at about 500 mbar. The mean of the ascent and descent profiles has been used for the winds. For temperature and humidity the higher value at a given pressure level has been used in order to minimize errors due to sensor time lag and 'wet bulb' effects (Taylor 1983).

The results presented here represent the mean of three to five sub-periods on a given day together with the standard deviation of the mean. The latter provides an estimate of the reliability of the result in the presence of measurement errors and natural variability over the meteorological triangle. An important assumption in these calculations is that the mean gradients are linear across the budget area. This may not be so in the presence of atmospheric fronts (Taylor & Guymer, this symposium), variations in sea surface temperature (Guymer *et al.*, this symposium), or mesoscale variability (Nicholls *et al.*, this symposium) not properly sampled by the radiosondes. However, comparison of values from different days (§ 5) gives some indication of the degree of confidence to be placed in the results.

(*b*) *Corrections to the surface pressure gradient*

The values of τ_x and τ_y initially calculated from the momentum budget appeared unrealistic in that the stresses increased with height. This has been assumed to be an error caused by inaccuracy in the surface pressure gradient in equation (4). Corrections to the surface pressure gradient have been calculated by assuming that τ_x and τ_y are both zero at some pressure level p_τ^*, defined as the lowest level satisfying the assumption that stress values above p_τ^* should be small. The resulting corrections are shown in table 2. The implied error in the pressure measurements is generally smaller than their accuracy, estimated by Macklin & Guymer (1980) as 0.2 mbar. Errors of this magnitude may be caused, for example, by airflow disturbance around the ships

PHILOSOPHICAL TRANSACTIONS OF THE ROYAL SOCIETY A MATHEMATICAL, PHYSICAL & ENGINEERING SCIENCES

TABLE 2. PRESSURE p_τ^* AT WHICH $\tau_x = \tau_y = 0$ WAS ASSUMED, AND THE PRESSURE GRADIENT CORRECTIONS Δp_x, Δp_y, EASTWARDS AND NORTHWARDS

day (1978)	surface pressure mbar	p_τ^* mbar	Δp_x mbar/200 km	Δp_y mbar/200 km
22 Aug.	1010	870	0.09	0.04
24 Aug.	1020	900	0.07	−0.12
25 Aug.	1025	950	0.14	−0.10
31 Aug.	1015	865	0.07	−0.03
1 Sep.	1010	850	−0.05	−0.27
mean	—	—	0.06	−0.10

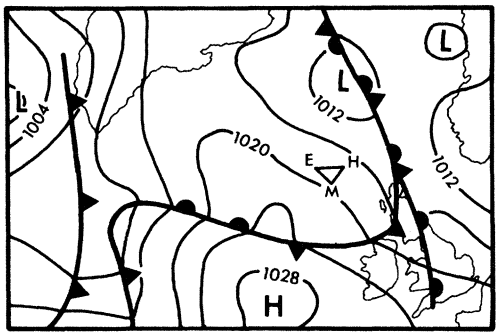

FIGURE 1. Synoptic situation at 12h00 G.M.T., 31 August 1978 adapted from the Daily Weather Report. The JASIN area is marked by the triangle with the ships indicated thus: E, *Gardline Endurer*; H, H.M.S. *Hecla*; M, R.V. *Meteor*.

and therefore might vary from day to day. The validity of these pressure corrections will be considered further in § 6.

4. 08h00–20h00 G.M.T. 31 AUGUST 1978

(*a*) *Synoptic situation*

Figure 1 shows the synoptic situation at 12h00 G.M.T. on 31 August 1978. The JASIN area was in a northwesterly airstream following the passage of an occluding frontal system during the previous night (Guymer *et al.*, this symposium). The JASIN radiosondes showed that, after a second weak front within the cold air, the boundary layer height was approximately constant at each ship with a small inversion slope over the area. This period, between 08h00 and 20h00 G.M.T., was well sampled by the radiosondes and represents an optimum period for budget calculations.

During the period, the near-surface wind speed was about 10 m s^{-1}, the sea–air temperature difference 0.5–1.0 K and the wet bulb depression about 2 K (Guymer & Taylor 1978). The observed clouds at *Endurer* and *Meteor* were predominantly stratocumulus ($C_L 5$) with some cumulus below ($C_L 8$), while at *Hecla* cumulus under stratocumulus ($C_L 8$) was more usual and slight rain showers were reported (see Meteorological Office (1977) for WMO cloud codes $C_L 5$, etc. used).

(*b*) *Mean boundary layer structure*

Figure 2*a* shows the mean profiles of Θ_v and q for each of the ships. Small vertical gradients within the subcloud and cloud layers contrast with large changes across the inversion layer. The inversion height, defined as the base of the layer of rapid humidity decrease, was highest at *Hecla* and lowest at *Endurer* with an overall mean value of 885 mbar. The maximum and minimum

inversion heights have been used to define the depth of the mean inversion layer, as shown in figure 2*a*. Note, however, that the actual inversion-layer depth, observed in a single radiosonde flight, was considerably smaller, being similar to or less than the 5 mbar resolution of the data. Thus the actual inversion should be considered as a sharp interface sloping in time and space between the limits shown. Budget values in the mean inversion layer represent a mean over this sloping interface and do not represent the vertical structure at any one point (see § 5*c*).

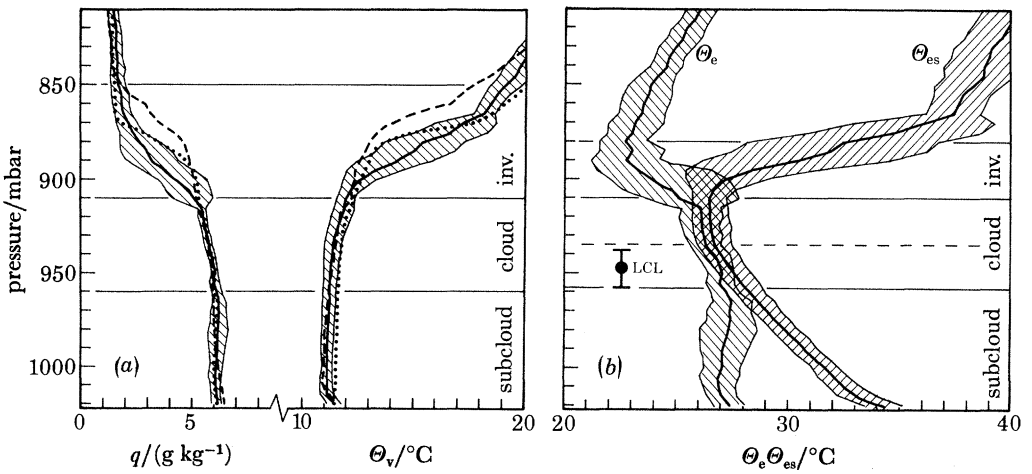

FIGURE 2. (*a*) Mean profiles of virtual potential temperature, Θ_v, and specific humidity, q, for radiosonde flights between 03h00 and 20h00 G.M.T., 31 August 1978. The curves represent 11 flights from *Endurer* (solid lines), 10 flights from *Hecla* (dashed lines) and 11 flights from *Meteor* (dotted lines). The standard deviation of individual profiles is shown for *Endurer* (shaded area), flights from the other ships showed similar variability. See text for the layer definitions.

(*b*) Mean profiles of equivalent potential temperature, Θ_e, and saturation equivalent potential temperature, Θ_{es}, for the *Endurer* flights shown in figure 2*a*. Also shown is the range of inversion heights at *Endurer*, the lifting condensation level, LCL, for subcloud-layer air and the lowest level at which the balloon entered the stratocumulus layer.

The mean structure of the cloud and subcloud layers is illustrated in figure 2*b* by profiles of Θ_e and Θ_{es} for the *Endurer* flights. Within the subcloud layer both Θ and q showed small mean increases with height, whereas q decreased in the cloud layer, resulting in a maximum in Θ_e at about 965 mbar. This may mark the limit of turbulent mixing originating from the sea surface, which Nicholls *et al.* (this symposium) found to extend to about $0.2\,u_*/f$ or, for this case, 957 mbar. The mean lifting condensation level (LCL) for subcloud-layer air, 948 mbar, would therefore have been above the level reached by turbulent mixing. However, the variability, $\pm$ 10 mbar, was such that condensation might sometimes occur at the subcloud-layer top. The decrease of Θ_e in the nearly saturated cloud layer suggests that the resulting cumulus clouds would rapidly extend up to the stratocumulus layer beneath the main inversion. The base of this layer, determined by observing the balloon entering the cloud, was about 935 mbar. The base of the lower cumulus and hence of the cloud layer was less readily determined. In the figures it has been marked as the lowest extent of the variation in LCL but this should only be considered as a guide.

Similar structure was observed at *Meteor*. At *Hecla*, however, q and Θ_e decreased between the surface and about 990 mbar and as a result the Θ_e maximum was less pronounced. The mean wind profiles at *Hecla* were also different (figure 3). *Endurer* and *Meteor* both showed relatively constant wind velocity in the subcloud and cloud layers, with wind speed increase and veering in the inversion layer. At *Hecla* there was a gradual increase of wind speed with height through the BL

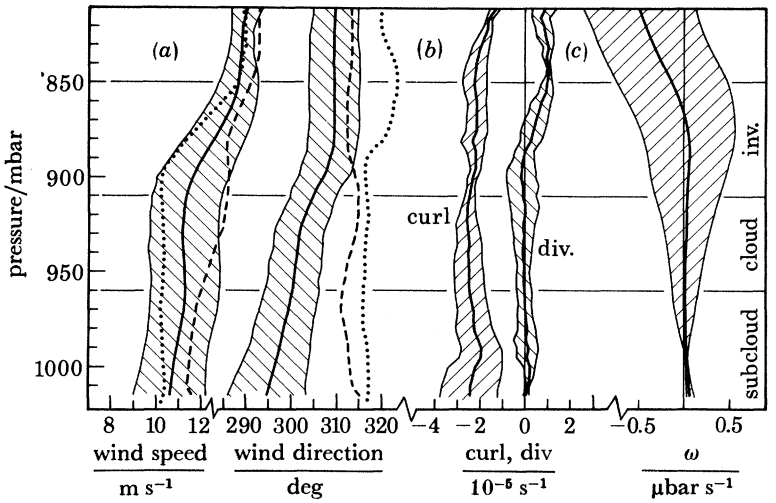

FIGURE 3. Mean profiles of (*a*) wind speed and direction corresponding to the profiles of figure 2*a*, (*b*) mean 200 km triangle values of horizontal divergence (div) and the vertical component of relative vorticity (curl) over the meteorological triangle, (*c*) the vertical motion ω. For div, curl, and ω the shaded region marks the standard deviation of the mean calculated from the individual four-hour budgets.

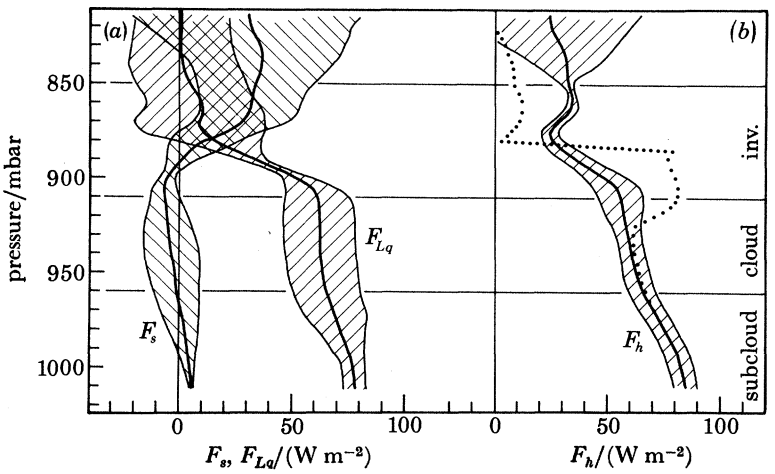

FIGURE 4. Mean profiles of the sub-grid-scale fluxes for 08h00–20h00 G.M.T., 31 August for (*a*) dry static energy, F_s, and latent energy F_{Lq} (radiation and condensation neglected) and (*b*) moist static energy, F_h, with a radiation estimate both neglected (solid line) and included (dotted line). The shaded regions indicate the standard deviation for the four-hour subperiod budgets.

with little change in wind direction. The cause of the differences at *Hecla* is not known; one possibility is that they were associated with the observed rain showers.

Figure 3 also shows the mean profiles of horizontal divergence and the vertical component of relative vorticity. The latter was anticyclonic and approximately constant with height. The divergence was small in the BL but increased at the top of the inversion layer. The resulting mean vertical motion ω was small and the vertical advection of momentum and thermodynamic energy was negligible within the boundary layer.

(*c*) *Thermodynamic energy budgets*

The calculated sub-grid-scale fluxes of dry static energy, F_s, and latent energy, F_{Lq}, shown in figure 4*a* are similar to those presented by previous authors for other regions (see, for example,

Augstein *et al.* 1973). The flux F_{Lq} was the most important (surface Bowen ratio = 0.08) within the BL. These fluxes have been inferred from the budget terms shown in table 3, in which the u direction is that of the surface wind. The lack of appreciable shear in wind direction meant that the v advections were negligible, as in general were the vertical advections, and the calculation of the flux divergence depended only on the local time changes and u advection.

TABLE 3. RATE OF CHANGE TERMS FOR DRY STATIC ENERGY, s, AND LATENT ENERGY, Lq, (in mW kg^{-1}) FOR 31 AUGUST 1978

(The inversion layer is shown as lower and upper halves. Significant terms are shown in bold type.)

layer (mbar)	$\frac{\partial s}{\partial t}$	$u\frac{\partial s}{\partial x}$	$v\frac{\partial s}{\partial y}$	$\omega\frac{\partial s}{\partial p}$	$\frac{\mathrm{D}s}{\mathrm{D}t}$	$\frac{\partial(Lq)}{\partial t}$	$u\frac{\partial(Lq)}{\partial x}$	$v\frac{\partial(Lq)}{\partial y}$	$\omega\frac{\partial(Lq)}{\partial p}$	$\frac{\mathrm{D}(Lq)}{\mathrm{D}t}$
subcloud (surface–960)	−12	**27**	−4	0	11	**24**	−2	1	0	**23**
cloud (955–910)	−7	18	−1	0	10	4	4	0	1	9
lower inv. (905–880)	17	**−83**	0	3	**−63**	−11	**180**	0	−15	**154**
upper inv. (875–850)	**−55**	**−25**	3	7	**−70**	**45**	0	−4	−9	**32**
free atmos. (845–810)	**−36**	**104**	8	**−31**	**45**	14	−20	−4	16	6

The small decrease of F_{Lq} in the subcloud layer was inferred from local moistening with time, otherwise F_{Lq} was nearly constant up to the inversion layer and near zero above. Thus most of the moisture flux from the sea surface was used in maintaining the slope of the inversion ($u\,\partial(Lq)/\partial x$ in table 3) although there was some moistening of the upper part of the inversion layer ($\partial(Lq)/\partial t$) despite the inversion height being nearly constant with time. Since ω was negligible in the BL, F_{Lq} represents the net vertical transport of latent energy. This is in contrast to trade wind results (Augstein *et al.* 1973; Holland & Rasmusson 1973) where the mean and sub-grid-scale transports were of similar order.

Despite the large variability, the mean F_s profile shows the expected behaviour with upward flux confined to the subcloud layer and downward flux to the cloud layer, the decrease being inferred from the u advection. Changes in the inversion layer due to the sloping inversion and cooling of the upper inversion with time imply an apparent upward F_s in the free atmosphere. This is reflected in the F_h profile (figure 4*b*), which also shows the effect of including a radiative heating estimate. The latter should be viewed with caution since it was based on a single 'representative' radiosonde flight from *Meteor*; a more accurate radiation estimate was prevented by the difficulty of specifying the cloud properties over the whole area. Nevertheless inclusion of radiative heating can clearly account for the upward F_s and F_h, which was otherwise inferred in the free atmosphere.

In the cloud layer much of the inferred F_s and F_{Lq} fluxes was probably due to condensation near the cloud-layer base, net upward transport of liquid water through the cloud layer, and evaporation at the cloud top (see, for example, Brümmer 1976). That the variability of F_s and F_{Lq} in the BL may have been caused by variation in such saturation processes is suggested by the smaller variability of the F_h profile, particularly within the cloud and inversion layers.

In summary, maintenance of the inversion slope in the downstream direction required the moistening and cooling of entrained air from the free atmosphere. The net addition of water vapour into the BL was by the flux from the sea surface; the loss of heat was by radiative cooling from the cloud top.

PHILOSOPHICAL TRANSACTIONS OF THE ROYAL SOCIETY A MATHEMATICAL, PHYSICAL & ENGINEERING SCIENCES

(*d*) *Momentum budget*

Table 4 shows the acceleration components for each of the layers, as for the thermodynamic energies both v and ω advections were negligible. Anticyclonic curvature of the wind field (figure 3) resulted in a large $u\,\partial v/\partial x$ acceleration, which was balanced by a geostrophic departure (figure 5*a*) such that the u component, and to a lesser extent the wind speed, were supergeostrophic through much of the BL.

TABLE 4. ACCELERATION TERMS/(10^{-5} m s^{-2}) FOR WIND COMPONENTS PARALLEL, u, AND NORMAL, v, TO THE SURFACE WIND FOR 31 AUGUST 1978

(Significant values are shown in bold type.)

layer (mbar)	$\frac{\partial u}{\partial t}$	$u\frac{\partial u}{\partial x}$	$v\frac{\partial u}{\partial y}$	$\omega\frac{\partial u}{\partial p}$	$\frac{\partial v}{\partial t}$	$u\frac{\partial v}{\partial x}$	$v\frac{\partial v}{\partial y}$	$\omega\frac{\partial v}{\partial p}$
subcloud (surface–960)	**3**	1	0	0	−3	**17**	0	0
cloud (955–910)	**4**	2	−1	0	−2	**14**	0	0
lower inv. (905–880)	**4**	**5**	0	0	0	**12**	0	0
upper inv. (875–850)	**4**	**4**	0	1	1	**20**	0	0
free atmos. (845–810)	1	0	0	0	2	**20**	0	0

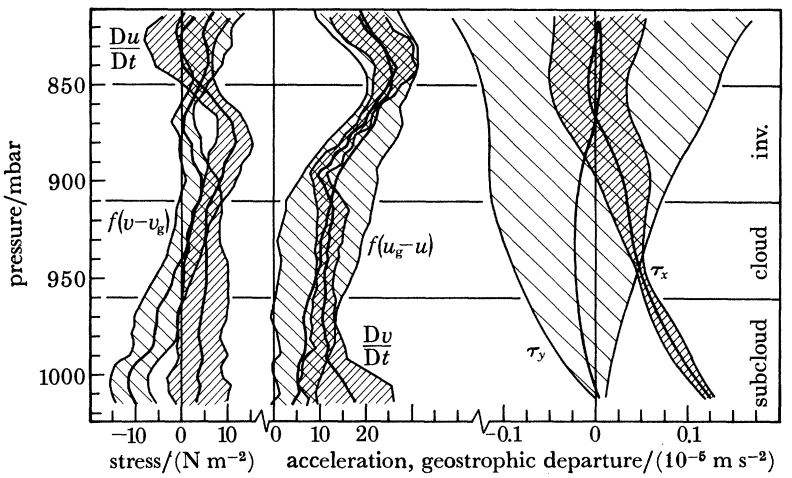

FIGURE 5. Mean profiles for 08h00–20h00 G.M.T., 31 August of the total accelerations, Du/Dt, Dv/Dt, the geostrophic departures, $f(v-v_g)$, $f(u_g-u)$ and the sub-grid-scale stress profiles τ_x, τ_y, where τ_x is in the direction of the mean surface stress. The shaded regions indicate the standard deviation for the four-hour subperiod budgets.

Significant variability in the $f(u_g-u)$ estimates resulted in great variability in the calculated τ_y profiles (figure 5*b*). However, τ_x was well defined and decreased in the subcloud layer to about 0.5 of the surface value. The stress profiles will be discussed in more detail in § 6.

5. COMPARISON OF FIVE DAYS

(*a*) *Synoptic situation*

The results from 31 August will in this section be compared with those for four other days. On 1 September the warm front, shown in figure 1, to the southwest of JASIN advanced toward the area. The synoptic development during these two days is described in more detail by Guymer *et al.* (this symposium). The two days 24 and 25 August (Taylor & Guymer, this symposium)

TABLE 5. SURFACE VALUES OF THE THERMODYNAMIC ENERGY FLUXES F_s, F_{Lq} AND F_h, AND SURFACE STRESS, τ_0, DERIVED FROM THE BULK AERODYNAMIC FORMULA; THE DIRECTION IS THAT FROM WHICH THE SURFACE WIND WAS BLOWING. ALSO SHOWN ARE THE BOWEN RATIO, THE MONIN–OBUKHOV LENGTH, $\mathscr{L}$, AND THE MOST FREQUENTLY REPORTED LOW CLOUD TYPES C_L†

day (1978)	budget period (G.M.T.)	F_s / W m^{-2}	F_{Lq} / W m^{-2}	F_h / W m^{-2}	Bowen ratio	$10^{-2}\tau_0$	direction / deg	$\mathscr{L}$ / km	C_L
22 Aug.	12h00–24h00	−1	24	23	−0.04	9.6	278	0.4	5+8
24 Aug.	00h00–24h00	−3	42	39	−0.07	9.5	276	22	5+8
25 Aug.	04h00–16h00	−1	15	14	−0.07	4.0	280	1.4	5
31 Aug.	08h00–20h00	6	73	79	0.08	12.5	309	0.3	5+8
1 Sept.	04h00–16h00	3	40	43	0.08	7.2	289	1.0	8+5+1

† Cloud types are indicated by standard codes (Meteorological Office 1977): C_L1, small cumulus; C_L5, stratocumulus; C_L8, cumulus and stratocumulus.

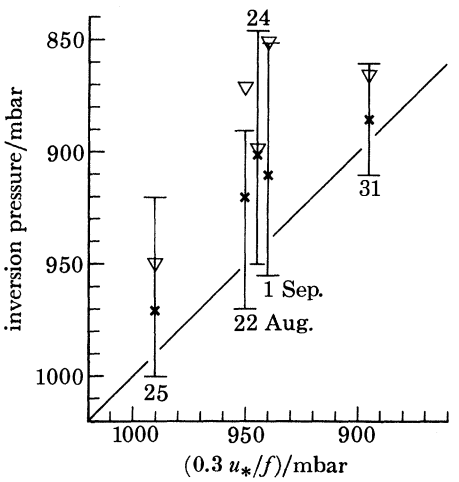

FIGURE 6. Inversion height against 0.3 u_*/f (in mbar) for each of the five budget days, 22, 24, 25, 31 July and 1 September. The crosses indicate the mean inversion height p_i^* from the relative humidity structure, the bars show the total range of observed values. The triangles indicate p_τ^*.

represented a similar situation except that the frontal region did not advance as far south of JASIN. On 22 August JASIN was in a westerly airstream (Pollard *et al.*, this symposium) with a weak occlusion clearing *Hecla* by midday.

To avoid the effect of frontal passages the budgets have been calculated for the periods shown in table 5, which lists the mean surface fluxes. These were greatest on 31 August. On each day the latent energy flux dominated (Bowen ratio ≈ 0.07) and the Monin–Obukhov length was similar to or greater than the depth of the subcloud layer. Near-neutral stability and mechanically generated turbulence in the Ekman layer were typical of JASIN (see, for example, Nicholls *et al.*, this symposium).

The mean, maximum and minimum inversion heights (as defined in § 4*b*) for each day are shown in figure 6. The minimum height corresponded to about 0.3 u_*/f. Compared with 31 August the BL was shallower on the other days and the inversion sloped significantly in both time and space resulting in a deeper mean inversion layer. The height, p_τ^*, at which $\tau_x = \tau_y = 0$ was assumed, is also shown in figure 6. This was chosen solely by reference to the stress profiles. However, in each case p_τ^* is in the region of the upper inversion layer, and hence plausible.

PHILOSOPHICAL TRANSACTIONS OF THE ROYAL SOCIETY A MATHEMATICAL, PHYSICAL & ENGINEERING SCIENCES

TABLE 6. MEAN DEPTH OF SUBCLOUD AND CLOUD LAYERS ON EACH DAY AND THE THERMODYNAMIC ENERGY GRADIENTS WITHIN THEM (POSITIVE UPWARDS). ALSO SHOWN IS THE APPROXIMATE MEAN EQUIVALENT POTENTIAL TEMPERATURE CHANGE ACROSS THE INVERSION, $\Delta\Theta_e$

	subcloud layer				cloud layer				
day (1978)	depth / mbar	$\partial s/\partial p$ / J kg^{-1} mbar^{-1}	$\partial(Lq)/\partial p$ / J kg^{-1} mbar^{-1}	$\partial h/\partial p$ / J kg^{-1} mbar^{-1}	depth / mbar	$\partial s/\partial p$ / J kg^{-1} mbar^{-1}	$\partial_{Lq}/\partial p$ / J kg^{-1} mbar^{-1}	$\partial h/\partial p$ / J kg^{-1} mbar^{-1}	$\Delta\Theta_e$ / K
22 Aug.	15	−30	42	35	30	18	−65	−48	−2
24 Aug.	30	3	−22	−18	30	15	−63	−48	−2
25 Aug.	10	−17	81	64	20	19	−56	−37	$-5\frac{1}{2}$
31 Aug.	55	1	−7	−5	50	20	−39	−19	−3
1 Sep.	25	−6	−4	−1	35	18	−70	−51	−2

TABLE 7. MEAN WIND GRADIENTS, VERTICAL RELATIVE VORTICITY, curl, HORIZONTAL DIVERGENCE, div, AND VERTICAL MOTION, ω, FOR MEAN SUBCLOUD AND CLOUD LAYERS. ALSO SHOWN IS THE MEAN VERTICAL MOTION AT THE MEAN INVERSION HEIGHT ω_{inv}

	subcloud layer					cloud layer					
day (1978)	$\partial u/\partial p$ / m s^{-1} mbar^{-1}	$\partial v/\partial p$ / m s^{-1} mbar^{-1}	curl / 10^{-6} s^{-1}	div / 10^{-6} s^{-1}	ω / μbar s^{-1}	$\partial u/\partial p$ / m s^{-1} mbar^{-1}	$\partial v/\partial p$ / m s^{-1} mbar^{-1}	curl / 10^{-6} s^{-1}	div / 10^{-6} s^{-1}	ω / μbar s^{-1}	ω_{inv} / μbar s^{-1}
22 Aug.	0.13	−0.03	−6	14	−0.2	−0.01	−0.03	−2	9	−0.5	−0.6
24 Aug.	0.05	−0.10	−17	14	−0.4	0.01	−0.05	−19	7	−0.8	−1.0
25 Aug.	0.04	−0.03	−22	1	−0.1	0.01	−0.03	−21	−6	0	0.3
31 Aug.	0.01	0	−23	1	0	0.01	−0.01	−25	−1	0	0.1
1 Sep.	0.01	0	−1	−2	0.1	0.02	−0.03	−4	−3	0.2	0.2

(*b*) *Mean boundary layer structure*

The mean thermodynamic energy profiles within the BL are represented in table 6 by the mean vertical gradients within the subcloud and cloud layers averaged over the three ships. Gradients in the subcloud layer were very variable for both s and Lq, and on both 22 and 25 August Lq increased with height. In the cloud layer the gradients were similar on each day, being between the moist and dry adiabatic values. The possibility of conditional instability is indicated by the decrease of h within the cloud layer and the decrease of Θ_e at the inversion. The latter was calculated from the mean $\Delta\Theta_e$ at each ship; for a given flight $\Delta\Theta_e$ would often be larger.

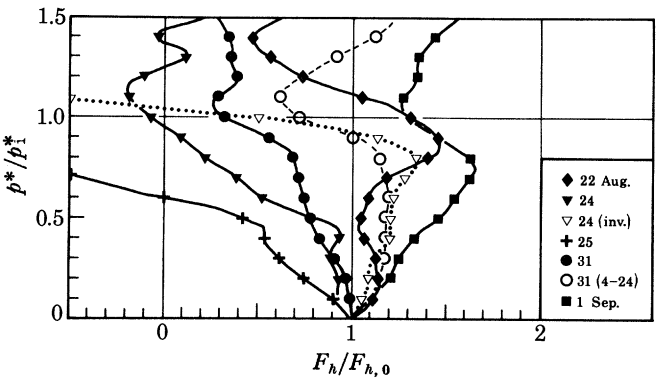

FIGURE 7. The mean sub-grid-scale moist static energy flux profiles, F_h normalized by the surface flux $F_{h,0}$ and the mean inversion height p_i^*, for each of the days shown. 24(inv.) indicates values for the 24 August normalized by the inversion height before averaging. 31(4–24) indicates values obtained by using all flights on the 31 August (04h00–24h00 G.M.T.). Note that the data intervals were considerably smaller than the spacing between the symbols, which are used only to differentiate between the curves.

Wind gradients (table 7) within the BL were generally small. The vorticity was anticyclonic of order 10^{-5} s^{-1}. Divergence within the BL was greatest on 22 and 24 August. The resulting ω values were generally less than 1 μbar s^{-1} ($\approx$ 1 cm s^{-1}) in magnitude.

(*c*) *Thermodynamic energy budgets*

As on 31 August the sub-grid-scale flux of latent energy, F_{Lq}, was dominant on each day. The resulting moist static energy flux profiles, F_h, are shown in figure 7 normalized by the surface flux and by the mean inversion level for each of the budget periods shown in table 5 (solid lines). On three days F_h was relatively constant up to the mean inversion height whereas on 24 and 25 August F_h decreased significantly above about $0.5\,p_i^*$. However, figure 6 shows that $0.5\,p_i^*$ approximately corresponds to the base of the mean inversion layer on these days. That the apparent decrease was due to averaging across the sloping inversion has been confirmed by normalizing the four-hour budget subperiod results on 24 August by the varying inversion height before forming the mean. The resulting profile (dotted line in figure 7) shows a slight increase of F_h up to $0.8\,p_i^*$. Different changes in the inversion height at each ship on the other days prevented use of this normalization technique. However, a method of budget calculation that takes into account the varying layer depths has been developed and will be described elsewhere (Günter & Olbrück 1983). It has been found to give physically more realistic flux profiles in cases of changing boundary layer depth but is at present more sensitive to measurement errors.

The near-constant inversion height on 31 August suggests that the F_h profile will be most realistic on that day and a further profile is shown (dashed line in figure 7) corresponding to the

whole day. This, along with the profiles for 22 and (normalized) 24 August and 1 September shows an increase of F_h in the BL by 10–12 W m^{-2} (26 W m^{-2} on 1 September). This was caused by an upward-increasing F_{Lq} suggesting that the sub-grid-scale processes were tending to dry out the BL for these budget periods.

TABLE 8. MEAN VALUES OF TOTAL ACCELERATION AND GEOSTROPHIC DEPARTURE TERMS/(10^{-5} m s^{-2}) IN EACH LAYER ON THE FIVE DAYS. ALSO SHOWN IS THE MEAN MAGNITUDE OF THE TERMS, THE MEAN, AND THE MEAN DIFFERENCE, THAT IS THE FRICTIONAL FORCE

	subcloud		cloud		inversion		free atmosphere	
day (1978)	Du/Dt	$f(v-v_g)$	Du/Dt	$f(v-v_g)$	Du/Dt	$f(v-v_g)$	Du/Dt	$f(v-v_g)$
22 Aug.	2	−25	1	−16	−1	−1	−6	13
24 Aug.	−2	−23	5	−2	15	11	28	10
25 Aug.	1	−9	3	−1	4	2	5	6
31 Aug.	4	−8	5	1	10	2	2	5
1 Sep.	0	−5	2	2	11	6	3	4
mean magnitude	2	14	3	4	8	4	9	8
mean	1	−14	3	−3	8	4	6	8
friction	15		6		4		−2	
	Dv/Dt	$f(u_g-u)$	Dv/Dt	$f(u_g-u)$	Dv/Dt	$f(u_g-u)$	Dv/Dt	$f(u_g-u)$
22 Aug.	−5	2	−2	4	−4	−6	−5	−9
24 Aug.	7	1	6	8	8	9	21	10
25 Aug.	12	1	7	4	6	5	17	10
31 Aug.	12	7	12	11	15	19	23	24
1 Sep.	9	−7	4	2	6	7	15	20
mean magnitude	9	4	6	6	8	9	16	15
mean	7	1	5	6	6	7	14	11
friction	6		−1		−1		3	

Above p_i^* the variability of the flux estimates increased greatly (see, for example, figure 4), giving unreliable F_h estimates in the free atmosphere. However, the mean value over all the periods, 19 ± 18 W m^{-2}, was of reasonable size to be ascribed to radiational heating (see, for example, Schmetz *et al.*, this symposium).

(*d*) *Momentum budget*

Table 8 shows the mean values of the total acceleration and geostrophic departure within each layer on the five days. In general the acceleration was of similar magnitude to the geostrophic departure with the numerical value of the two becoming similar as the stress diminished with height. As a result the maximum geostrophic departure in the free atmosphere was often similar to or even greater than that at the surface. The slow change in the overall synoptic situation (Pollard *et al.*, this symposium) meant that the accelerations would not become negligible even if averaged over the five days.

The resulting stress profiles are shown in figure 8 normalized by τ_0 and p_i^*. The τ_y values are maximum in amplitude at about 0.5 p_i^* and negative (upward momentum transfer) except on 22 August and in the cloud layer on 24 August. The variability was generally less for τ_y for days other than 31 August and more for the τ_x profiles. The latter were evenly distributed about the 31 August profile (§4*d*).

(*e*) *Eddy viscosity*

Approximate values of eddy viscosity are shown in table 9. In general the values could be defined through most of the BL except in the subcloud layer on 31 August and for K_v in parts of the cloud layer. The only significant counter-gradient transfers implied by the flux profiles were

on 22 August and in the cloud layer on 24 August. Eddy viscosity values were significantly greater on 31 August than on the other days, but all values were within the range found by previous authors (see, for example, Roll 1965).

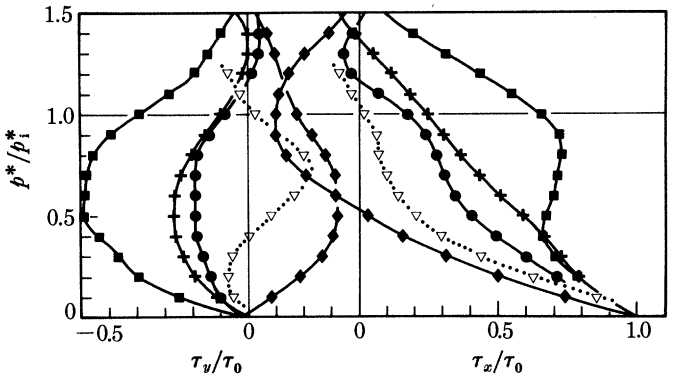

FIGURE 8. Stress profiles normalized by the surface stress τ_0 and the mean inversion height p_i^*. See figure 7 for key to symbols.

TABLE 9. APPROXIMATE VALUES OF EDDY VISCOSITY/($m^2\ s^{-1}$) WITHIN THE BL

(Negative (counter-gradient) values are shown in bold type. The values shown were estimated from profile plots ignoring regions in which small vertical gradients resulted in large ill defined eddy viscosity values being ignored (see text). Each eddy viscosity, K, refers to the variable shown by the subscript.)

day (1978)	K_u	K_v	K_s	K_{La}	K_h
22 Aug.	**−50 → 20**	**−20**	**−5**	5	10
24 Aug.	30	**0 → −20**	5	10	5
25 Aug.	10	5	5	0	0
31 Aug.	50 → 100	50 → 100	5	50	40
1 Sep.	40	20	**0 → −5**	10	10

6. DISCUSSION

The thermodynamic energy flux profiles (§§ 4*c*, 5*c*) were similar to those found previously by, for example, Holland & Rasmusson (1973) or Augstein *et al.* (1973), suggesting that the structure of the JASIN boundary layer was determined by similar physical processes to those operating in lower latitudes. However, the momentum budget results show differences that require discussion.

Previous studies of inversion-capped boundary layers (Holland & Rasmusson 1973; Brümmer 1976; Nitta & So 1980) found τ_x decreased rapidly in the subcloud layer, being less than 0.2 τ_0 at the condensation level. Nicholls *et al.* (this symposium) found, for JASIN, that turbulent momentum transfer become small at about 0.2 u_*/f, corresponding to the region of the condensation level, or 0.5 p_i^* in figure 8. However, only two cases in the present study show small τ_x at this level (figure 8). Two points must be made. Firstly, that τ_x decreases to zero in these results is solely due to the pressure corrections (§ 3*b*). However, forcing $\tau_x = 0$ at the LCL would have required unreasonably large surface pressure corrections and would have resulted in very large stress values in the cloud and inversion layers. Secondly, it has to be admitted that the variability of the stress profiles increased greatly above about 0.3 p_i^* and the observed stress at 0.5 p_i^* may not be significant on 25 August and 1 September. Nevertheless, the values on 31 August are significant. The quasi-stationary and horizontally uniform conditions on this day gave the most reliable budget estimates and the τ_x profile was well defined (figure 5).

In the trade-wind studies, transport of u momentum across a u component maximum in the subcloud layer and significant frictional forces, particularly in the v direction, within the cloud layer implied convective momentum transport in both subcloud and cloud layers (Brümmer *et al.* 1974; Brümmer 1976). Increased stress was observed during JASIN in both subcloud and cloud layers when a cumulus cloud field was present under the stratocumulus (Nicholls *et al.*, this symposium). It is possible that convective momentum transport, occurring intermittently over the area and period of the budget calculations, could account for the significant τ_x values observed in the cloud layer. The maximum mean value required would be less than 10 % of the maximum cloud-layer stress value measured by Pennell & LeMone (1974).

If the mean τ_x profiles on days other than 31 August are representative then 22 August was most similar to the trade-wind observations; τ_x decreased to zero near the cloud-layer base and there was a u component maximum at a low level such that the negative τ_x in the cloud layer represented down gradient momentum transport. On this day and on 24 August, when τ_x at the cloud base was also small, there was significant downward ω within the BL (table 8). The small or upward ω on the other days is in contrast to the observations of all the previous authors quoted where significant downward vertical motion was observed in the cloud and upper subcloud layers. The resulting difference in the total mean vertical thermodynamic fluxes was noted previously (§ 4*c*).

If the τ_y profiles are to be believed then the maximum amplitude occurred near the subcloud-layer top. However, in view of the large variability (see, for example, § 4*d*) only the value on 1 September is significantly non-zero. The difficulty of obtaining reliable τ_y estimates by budget techniques has been noted by Brümmer (1976) and ascribed to the difficulty of obtaining the stress gradient as a small difference between coriolis and pressure gradient forces, both of which are large for this component.

A significant difference between the JASIN observations and those for trade-wind areas is that in JASIN the acceleration terms were significant within the BL. The consequences of this in a similar midlatitude area have been discussed by Augstein & Heinricy (1976) using the treatment of Mahrt (1975).

7. Summary

The JASIN BL observations presented show a near-neutral subcloud layer capped by a conditionally unstable cloud layer that typically contained cumulus clouds under a stratocumulus layer. Momentum transfer was by mechanical mixing in the subcloud layer but significant convective momentum transfer is suggested in the upper subcloud and cloud layers. Accelerations were significant in the BL on all occasions. However, terms involving the mean vertical motion were small.

Latent energy was the dominant sub-grid-scale thermodynamic flux and was relatively constant from the surface to the main inversion at the cloud-layer top. Sometimes an increase with height was observed suggesting that the sub-grid-scale fluxes acted to dry the BL. The residual of the moist static energy budget at the cloud-layer top was of the order of the estimated radiative cooling. Thus on 31 August, chosen for detailed study, the increase in inversion height along the surface wind direction was maintained by moistening from the sea surface together with radiative cooling from the cloud top.

Despite some differences, the JASIN observations showed many similarities to the BLs of lower latitudes, suggesting that, for the inversion-capped BLs chosen, similar physical processes were

PHILOSOPHICAL TRANSACTIONS OF THE ROYAL SOCIETY A MATHEMATICAL, PHYSICAL & ENGINEERING SCIENCES

operating. The main characteristic of the midlatitude atmosphere is its variability. In a later study it is hoped to extend the analysis to cases in which the BL structure was significantly different to that presented here.

References

Augstein, E. & Heinricy, D. 1976 Actual and geostrophic wind relationships in an accelerated marine atmospheric boundary layer. *Beitr. Phys. Atmos.* **49**, 55–68.

Augstein, E., Riehl, H., Ostapoff, F. & Wagner, V. 1973 Mass and energy transports in an undisturbed Atlantic Trade Wind flow. *Mon. Weath. Rev.* **101**, 101–111.

Brümmer, B., Augstein, E. & Riehl, H. 1974 On the low-level wind structure in the Atlantic trade. *Q. Jl R. met. Soc.* **100**, 109–121.

Brümmer, B. 1976 The kinematics, dynamics and kinetic energy budget of the trade wind flow over the Atlantic Ocean. *Meteor Forsch.* B **11**, 1–24.

Brümmer, B. 1978 Mass and energy budgets of a 1 km high atmospheric box over the GATE C-scale triangle during undisturbed and disturbed weather conditions. *J. atmos. Sci.* **35**, 997–1011.

Charnock, H., Francis, J. D. R. & Sheppard, P. A. 1956 An investigation of wind structure in the Trades, Anegada, 1953. *Phil. Trans. R. Soc. Lond.* A **249**, 179–234.

Günter, H. & Olbrück, G. 1983 Comparison of budget analysis on variable and fixed layers including temporal and spatial variations of characteristic meteorological layers. (In preparation.)

Guymer, T. H. & Taylor, P. K. 1978 Preliminary assessment of shipboard meteorological program. JASIN news, no. 11.

Holland, J. Z. & Rasmussen, E. M. 1973 Measurements of atmospheric mass, energy and momentum budgets over a 500 kilometre square of tropical ocean. *Mon. Weath. Rev.* **101**, 11–55.

Large, W. G. & Pond, S. 1982 Sensible and latent heat flux measurements over the ocean. *J. phys. Oceanogr.* **12**, 464–482.

Macklin, S. A. & Guymer, T. H. 1980 Inter-platform comparisons of JASIN WMO observations. JASIN news, no. 15.

Meteorological Office 1977 *Ships' code and decode book*, 9th edn. (62 pp). London: H.M.S.O.

Mahrt, L. 1975 The influence of momentum advections on a well-mixed layer. *Q. Jl R. met. Soc.* **101**, 1–11.

Nitta, T. & Esbensen, S. 1974 Heat and moisture budget analysis using BOMEX data. *Mon. Weath. Rev.* **102**, 17–28.

Nitta, Ts. & So, S. S. 1980 Structure and heat, moisture and momentum budgets of a convective mixed layer during AMTEX'75. *J. met. Soc. Japan*, Ser. II. **58**, 378–393.

Pennell, W. T. & LeMone, M. A. 1974 An experimental study of turbulence structure in the fair weather trade wind boundary layer. *J. atmos. Sci.* **31**, 1308–1323.

Roach, W. T. & Slingo, A. 1979 A high resolution infrared radiative transfer scheme to study the interaction of radiation and cloud. *Q. Jl R. met. Soc.* **105**, 603–614.

Roll, H. U. 1965 *Physics of the marine atmosphere* (426 pp.). New York: Academic Press.

Sheppard, P. A., Charnock, H. & Francis, J. R. D. 1952 Observations of the westerlies over the sea. *Q. Jl R. met. Soc.* **78**, 563–582.

Sheppard, P. A. & Omar, M. H. 1952 The wind stress over the ocean from observations in the Trades. *Q. Jl R. met. Soc.* **78**, 583–589.

Slingo, A. & Schrecker, H. M. 1982 On the shortwave radiative properties of stratiform water clouds. *Q. Jl R. met. Soc.* **108**, 407–426.

Taylor, P. K. 1975 The JASIN radiosonde observations. In *Plans for the Joint Air–Sea Interaction experiments JASIN 1977 and 1978*, pp. 89–98. London: The Royal Society.

Taylor, P. K. 1983 JASIN Radiosonde Data: Processing and budget calculation. I.O.S. report, Institute of Oceanographic Sciences, Wormley, Surrey. (In preparation.)

PHILOSOPHICAL TRANSACTIONS OF THE ROYAL SOCIETY A MATHEMATICAL, PHYSICAL & ENGINEERING SCIENCES